NASA CONTRACTOR REPORT

NASA CR-542

NASA CR-542

PILOT DESCRIBING FUNCTION MEASUREMENTS IN A MULTILOOP TASK

by R. L. Stapleford, D. T. McRuer, and R. Magdaleno

Prepared by

SYSTEMS TECHNOLOGY, INC.

Hawthorne, Calif.

for Ames Research Center

NATIONAL AERONAUTICS AND SPACE ADMINISTRATION • WASHINGTON, D. C. • AUGUST 1966

NASA CR-542

PILOT DESCRIBING FUNCTION MEASUREMENTS IN A MULTILOOP TASK

By R. L. Stapleford, D. T. McRuer, and R. Magdaleno

Prepared under Contract No. NAS 2-1868-3 by
SYSTEMS TECHNOLOGY, INC.
Hawthorne, Calif.

for Ames Research Center

NATIONAL AERONAUTICS AND SPACE ADMINISTRATION

For sale by the Clearinghouse for Federal Scientific and Technical Information
Springfield, Virginia 22151 – Price $2.00

PILOT DESCRIBING FUNCTION MEASUREMENTS IN A MULTILOOP TASK

INTRODUCTION

As an element in a control system the human pilot operates, in general, in a nonlinear and time-varying manner. In many situations, however, his on-the-average responses can be represented by a quasi-linear model such as that shown in Fig. 1. The describing function component of the quasi-linear model gives that portion of the pilot response which is linearly related to the system input. The remnant is then the remainder of his response, i.e., that portion which is not correlated linearly with the command input.

For single-loop compensatory tracking situations the quasi-linear model is well developed; the most detailed recent treatment is provided in Ref. 1. Current research activities are directed at expanding the model in several areas — pursuit tracking, multiloop control tasks, and multimodal pilot inputs. The work reported in this paper deals with the expansion to multiloop situations.

At the outset of this program there had been several investigations in which human operator describing function measurements had been made in multiaxis situations (Refs. 7–9). In these studies the assumed (for data analysis purposes) and appropriate (based on data results) block diagram structure of the pilot/vehicle system was that shown in Fig. 2. Such a system can be termed "multiple single-loop," and the determination of the operator's describing function for each of the loops is quite simple, i.e.,

$$Y_{p_1} = \frac{\Phi_{i_1 c_1}}{\Phi_{i_1 e_1}} \tag{1}$$

$$Y_{p_2} = \frac{\Phi_{i_2 c_2}}{\Phi_{i_2 e_2}} \tag{2}$$

where $\Phi_{i_1 c_1}$ is the cross-spectral density between i_1 and c_1, etc.

Multiloop systems differ considerably from multiple single-loop systems, and represent a higher level of pilot/vehicle complexity. Examples of multiloop systems, with a classification based on the degree of coupling in the human controller, are shown in Fig. 3. The fundamental distinction between these and the multiple single-loop systems mentioned above is in the interaxis coupling inherent in the controlled-element dynamics. It is this kind of system which is of central interest here. Until the present experimental series there were no human operator describing function data available for such situations.

In spite of the data deficiency, pilot models for multiloop situations, based on a rational extension of single-loop results, have been in use for several years. Some of these have been quite successful in a number of applications, e.g., Refs. 2–6. Nonetheless, questions and uncertainties uncovered in these application studies have provided both incentive and context for experimental measurements of pilot dynamics in multiloop manual control systems. As a result, the experimental program described here was undertaken to provide data essential for the development of detailed adjustment rules, loop closure criteria, and other aspects of model refinement.

DESCRIBING FUNCTION MEASUREMENTS FOR MULTILOOP SYSTEMS

It can be shown that, in general, the number of measurable pilot describing functions is equal to the number of uncorrelated inputs times the number of pilot outputs or controls. For example, with the two inputs and two pilot outputs of the cross-fed multipoint controller (Fig. 3c) the equations for the pilot outputs are:

$$c_1 = Y_{p_{11}} e_1 + Y_{p_{12}} e_2 + n_1 \tag{3}$$

$$c_2 = Y_{p_{21}} e_1 + Y_{p_{22}} e_2 + n_2 \tag{4}$$

By taking the cross-spectra of the quantities in Eqs. 3 and 4 with each input, one obtains four equations of the form:

$$\Phi_{i_i c_j} = Y_{p_{j1}} \Phi_{i_i e_1} + Y_{p_{j2}} \Phi_{i_i e_2} \quad ; \quad i, j = 1, 2 \tag{5}$$

These can, in principle, be solved for the four (two uncorrelated inputs times two pilot outputs) describing functions $Y_{p_{11}}$, $Y_{p_{12}}$, etc.

Two of the four equations involve cross-spectra with the first input and the other two equations contain cross-spectra based on the second input. When the inputs are composed of sums of sine waves, they are uncorrelated only if their components are at different frequencies. Consequently, the four cross-spectral equations cannot be evaluated at the same frequencies. To solve the four equations simultaneously, it would be necessary to do one of the following:

- Interpolate the cross-spectral measurements to obtain values of the cross-spectra at the same frequencies for all four equations.
- Interchange the frequencies of the inputs and rerun the experiment so that data are available at the same frequencies for all the cross-spectra.

If, on the other hand, the pilot crossfeeds, $Y_{p_{12}}$ and $Y_{p_{21}}$, were not present, then this problem would be eliminated. In fact, because each "pilot box" in this direct multipoint controller is characterized by one input and one output, only one system input would be needed to determine the two pilot describing

functions. These would be given by the simple relationships

$$Y_{p_{11}} = \frac{\Phi_{ic_1}}{\Phi_{ie_1}} \tag{6}$$

$$Y_{p_{22}} = \frac{\Phi_{ic_2}}{\Phi_{ie_2}} \tag{7}$$

Intermediate between the direct multipoint and cross-fed multipoint controllers is a system wherein only one crossfeed is present. This is shown in Fig. 4 with the crossfeed Y_{cf} shifted to the output of the series pilot box. In terms of the cross-fed multipoint controller quantities, Y_{cf} is $Y_{p_{21}}/Y_{p_{11}}$. With only one input, $Y_{p_{11}}$ can still be determined explicitly because Eq. 6 still holds. The cross-spectral ratio of Eq. 7, however, no longer gives $Y_{p_{22}}$ explicitly; instead, this cross-spectral ratio contains both $Y_{p_{22}}$ and $Y_{p_{cf}}$, i.e.,

$$\frac{\Phi_{ic_2}}{\Phi_{ie_2}} = \frac{Y_{p_{22}}\left(\frac{r_2}{c_1}\right) + Y_{p_{cf}}}{\left(\frac{r_2}{c_1}\right) + Y_{p_{cf}}\left(\frac{r_2}{c_2}\right)} \tag{8}$$

where r_2/c_1 and r_2/c_2 are vehicle open-loop transfer functions. Consequently, the effect of the crossfeed cannot be separated from that of the loop closure, except implicitly, if the task involves but one forcing function.

From the standpoint of evolutionary development of pilot describing function data, the ideal experimental situation at this pioneering stage would be the direct multipoint controller with one forcing function. This would constitute a net advance over previous studies without the necessity of a complicating and perhaps unrealistic secondary input. On a more tangible and practical level, any multiloop experiments are fundamentally restricted in scope by the equipment and data reduction apparatus available. In our particular situation this consideration made single-input tasks most desirable. Thus an important implicit criterion in our control task selection was to avoid controlled elements which demanded $Y_{p_{12}}$ and $Y_{p_{21}}$ crossfeeds for their control. Ideally, neither crossfeed should be present, although this was recognized as perhaps too drastic a departure from realism. Even with just one command input the presence of crossfeed can be detected readily from the cross-spectral measurements when these are compared with analytical predictions, and some insight can be gained into the nature of the likely crossfeed by implicit techniques. Consequently, our consideration of measurement and analysis limitations suggested that the control task selected involve

- A single forcing function
- A controlled element which ideally would be controlled as a direct multipoint controller, or which, at worst, required no more than one crossfeed in the human pilot.

CONTROL TASK DESCRIPTION

Selection Criteria

As a first step in experimental planning several criteria were established to guide the selection of the specific control tasks to be used in the experiments. The first two criteria are noted immediately above. To these were added the following:

- At least two versions of controlled-element dynamics are needed, corresponding to single-loop and multiloop control, respectively.
    - For the single-loop task the controlled-element dynamics should be similar to those of the outer loop in the multiloop situation so that the two conditions can be compared. The dynamics should also be similar to those of previous single-loop experiments (e.g., Ref. 1) to allow a tie-in with previous data.
    - The multiloop configuration(s) should be such that direct control of the command input is impossible without the addition of a secondary or inner loop. Ideally, the dynamics should be such that with these loops closed by the pilot the resulting outer loop characteristics are similar to those of the single-loop version.
- For the multiloop task there should be at least two inner loop closure possibilities available to the pilot so that the feedback selection hypothesis (Ref. 13) can be tested. This hypothesis states that given a number of inputs and possible outputs, the pilot will select those feedbacks which give him the best dynamic performance with least pilot effort. This can be demonstrated by having two inner loop possibilities which differ markedly in their performance potential.
- To the extent possible, the controlled-element dynamics should impose a moderate constraint on the form of the pilot describing functions in each of the two channels. This serves to reduce the variability in the measurements and the number of runs required to obtain accurate data (Ref. 1).

Controlled-Element Description

After an extensive investigation of several possible vehicle control tasks, an aircraft control situation consisting of a bank angle tracking task was selected. Figure 5 shows the control situation and the vehicle dynamic equations. A bank angle command was the system input, and the difference between that command and the actual bank angle of the airplane was displayed to the pilot along with the aircraft yaw rate. The pilot could then use the ailerons and the rudders to control the vehicle dynamics, which were simulated on an analog computer.

Now, conventionally, bank angle tracking is a single-loop task for aircraft with good characteristics. Any configuration which exhibits such good handling qualities, and which also has dynamics in the crossover region which are similar to some set previously tested (Ref. 1), would be suitable for the single-loop baseline condition. For the multiloop configuration, the pilot can be forced into multiloop behavior by making the dutch roll mode dynamically unstable. This can be done in such a way that there is no equalization which the pilot can adopt to allow him to stabilize the dutch roll mode with only a bank-angle-to-aileron closure. In fact, by judicious selection of the unstable vehicle characteristics the dutch roll mode can be made slightly more unstable by the pilot closure of this loop. This is clearly seen in the root locus sketch of Fig. 6, which shows the closed-loop roots resulting from a bank-angle-to-aileron loop closure with pilot behavior approximated by a gain and transport lag describing function.*

One piloting technique for control of this vehicle is the use of a yaw-rate-to-rudder loop to stabilize the dutch roll mode and then a bank-angle-to-aileron closure to perform the tracking task. The effects of this inner and outer loop are shown in the root locus sketches of Fig. 7, again with gain and transport lag pilot elements. The inner loop yaw-rate-to-rudder feedback has the effect not only of stabilizing the dutch roll mode but also of shifting the bank angle zero. The outer loop closure, Fig. 7b, is therefore very simple to achieve. (In fact, the outer open-loop characteristics illustrated here are approximately those desired for the single-loop configuration.)

An alternate possibility to control the dutch roll instability is for the pilot to use bank angle and yaw rate closures with ailerons alone. This second technique is quite inferior to the first as regards performance. The nature of these closures is shown in the root locus sketches of Fig. 8. The yaw-rate-to-aileron closure can stabilize the dutch roll mode, but the bank angle closure destabilizes it such that attainable system bandwidth is severely limited. Consequently, tracking performance using the second technique is very inferior to that with the yaw-rate-to-rudder inner loop.

The performance obtainable by the yaw-rate-to-aileron plus bank-angle-to-aileron control technique can be altered considerably by varying the stability derivative N_p', which is the amount of yaw acceleration which is produced by a unit rolling velocity. This is shown in the root locus sketches of Fig. 9. When N_p' is increased, the complex zeros of the yaw-rate-to-aileron transfer function are reduced in frequency so that more damping of the dutch roll can be obtained with the bank-angle-to-aileron closure. N_p' is also an important cause of cross-coupling between the rolling and yawing degrees of freedom and, as will be discussed further below, this consideration was also important in setting up the final configurations.

---

*The actual pre-experiment analyses, conducted to guide the selection of controlled-element details, were performed using the more complex human pilot mathematical models of Ref. 1. The gain and transport lag models are suitable only for oversimplified qualitative descriptions. These are all that are required at this point.

PRELIMINARY EXPERIMENTS

Although the criteria and considerations outlined above were sufficient to establish the general characteristics of the controlled elements in some detail, there were still several loose ends and specifics which required resolution before the final experimental configurations could be established. To this end some preliminary experiments, in which no measurements of pilot describing functions were taken, were performed in the STI simulator facility. The objectives of these experiments were to

- Finalize the specific details of the configurations to be used in the main experimental program (e.g., N'_p and dutch roll damping ratio)
- Verify the general qualitative nature of the pre-experimental analyses and verify that pilot behavior would be of the type postulated
- Check the scaling and the gains for both the display and the controls
- Check the possibility of display sampling.

The experimental setup consisted of a fixed-base cockpit, an analog computer to simulate the equations of motion, and a cathode ray tube for the display. The displayed quantities were bank angle error, which was represented by the difference between a fixed and a rotating line, and yaw rate, which was represented by the horizontal displacement of a small spot (see Fig. 10). In terms of a real-flight situation the moving line in Fig. 10 represents the horizon, and this part of the display is essentially an inside-out bank angle attitude indicator. The yaw rate display was scaled so that the motion of the spot corresponded to that of the top of the turn needle in a conventional bank-and-turn indicator.

For both the preliminary and main experiments the instructions to the pilots were to minimize the bank angle error using whatever control technique they chose. When initially confronted with an unstable configuration, the pilots found that they could control the bank angle error very well for a few seconds using only the ailerons. Then, as time advanced, they would notice that the yaw rate spot oscillated with an ever-increasing amplitude, although this did not seriously affect the bank angle tracking until the yaw rate got rather large. At this point the bank angle tracking would rapidly deteriorate so as to make recovery almost impossible. All subjects soon learned that the best technique was to simultaneously track yaw rate with rudder and bank angle with aileron, and they would attempt to keep the yaw rate very small to avoid the problem of trying to recover once it got very large.

The yaw rate seen by the pilot is primarily a result of the excitation of the dutch roll mode, which is more or less a nuisance mode in that the pilot is not trying to use it to control his bank angle although he is, inadvertently, exciting it in the process of trying to track the bank angle command. This excitation comes primarily from two aerodynamic cross-coupling sources — the yaw acceleration produced by the ailerons and the yaw acceleration produced by

roll rate as the aircraft is rolled back and forth to follow the command. These correspond to $N'_{\delta_a}\delta_a$ and $N'_p p$, respectively, in the vehicle equations of motion (Fig. 5). As already noted, an increase in N'_p increases the excitation of the dutch roll mode and at the same time improves the performance potential of aileron-alone control. It was, accordingly, a major variable in the preliminary experiments in the evolution of final configurations which were qualitatively adequate in terms of the criteria set forth in the last section.

The preliminary experiments served all their purposes in the resolution of fine points. They also provided more important and general results, which can be summarized as follows:

- The roll control task had clear primacy, with inner loop stabilization a necessity to accomplish the outer loop task. There was no apparent tendency, or need, to cross-feed rudder to aileron.

- No evidences of display sampling were noted. This is based on the reports of the subjects and from visual observations of eye movements. The display was such that both bank angle and yaw rate could be observed simultaneously through the use of parafoveal vision.

- The bank-angle- and yaw-rate-to-aileron technique was found to be possible but very inferior to the yaw-rate-to-rudder and bank-angle-to-aileron technique. Consequently, the subjects would use the former only if instructed not to use the rudder pedals. Given a choice, the subjects would always adopt the yaw-rate-to-rudder and bank-angle-to-aileron technique regardless of the value of N'_p.

- A small value of N'_p was desirable to avoid yaw rate scaling problems in the display and computer. Small values of N'_p were also desirable to minimize the possibilities of control crossfeed. With large values of N'_p the subjects tended to use an aileron-to-rudder crossfeed to reduce the excitation of the dutch roll mode produced by the bank angle tracking.

On the basis of these preliminary experiments, three controlled-element configurations were selected to be run in the main set of experiments. The only variable between configurations was the derivative N'_r, which could be set to give the several levels of dutch roll damping required. The complete set of vehicle dynamic parameters is given in Appendix A.

N'_p was set to the low value of 0.02 sec^{-1} for all configurations. In anticipation of some of the later results, it is worth noting that with this value in the preliminary experiments the impressions of the subjects regarding control crossfeed were divided. One subject claimed to be using some aileron-to-rudder crossfeed, whereas the other was sure that he was not.

MAIN EXPERIMENTS

Task Variables

As a result of the preliminary experiments, three basic sets of controlled-element dynamics were evolved. These corresponded to three different levels of dutch roll damping, listed in Table I as Configurations A, B (D, E), and C. The roll subsidence mode is the same for all configurations, and was selected to be compatible with good rolling characteristics, as indicated by Ref. 11. The spiral mode and dutch roll undamped natural frequency are slightly different for the three configurations. These are incidental consequences of the changes in N'_r used to create the variation in dutch roll damping ratio.

Configuration A has a stable dutch roll, so an inner loop closure is not necessary. The characteristics of this configuration in the region of system crossover approximate the properties of other simpler systems already tested and reported in Ref. 1. Thus, the configuration can be used to provide a tie-in with these previous data. It also provides a reference for comparison with the cases in which the pilot was forced to use an inner loop. Configuration B (D and E) is just unstable enough to force the pilot to adopt multiloop control, whereas Configuration C has an instability level near the maximum controllable by the pilot. In fact, several practice runs were required before this configuration could be controlled at all for the four-minute run length used. These three controlled-element variations therefore provide a rather large range of variation of dutch roll damping and of required multiloop control activity.

The forcing function task variable was made up of a sum of ten sine waves with frequencies which were more or less equally spaced logarithmically across the measurement bandwidth. The vast majority of the input power was of a low frequency nature, achieved by setting the lower frequencies at one amplitude and the higher frequencies at an amplitude one-tenth that of the lower frequency waves. The total effect of all was an rms forcing function amplitude of 11 deg. The bandwidth of the input refers to the highest frequency of the large amplitude waves. For the controlled-element variations tested in Configurations A, B, and C this was set at 1.6 rad/sec, which corresponds approximately to the $\omega_1 = 1.5$ augmented rectangular forcing function used in the Ref. 1 experiments.

In addition to the controlled-element variations with fixed forcing function bandwidth, a complementary series was set forth using a fixed controlled element and three controlled-element bandwidths. This series is obtained from Configurations D, B, and E. The objective of this series was to determine whether the variations of describing function with input bandwidth observed in Ref. 1 for single-loop tasks had their analog in multiloop situations.

Measurements taken during the experiments consisted of average performance measures, pilot ratings, and cross-spectral data. The performance measures included mean-squared bank angle tracking error, $\overline{\varphi_e^2}$, and mean-squared yawing velocity, $\overline{r^2}$. The cross-spectral data were obtained using much of the equipment and techniques previously employed in the single-loop experiments of Ref. 1. To make the cross-spectral measurements, advantage was taken of the sum-of-sinusoid forcing function. Component sinusoids were used as references in conjunction with pilot outputs or other system parameters as signals into a watthour-meter analyzer. In this equipment the real and imaginary parts at a particular input frequency are obtained by using a component of the input and this component

shifted 90 deg in phase as reference signals to two watthour meters. The signal being cross-correlated with the input, e.g., the pilot output, system error, etc., makes up the other input to the meters. The watthour meters then perform the cross-spectral analysis functions of multiplication and integration, resulting in measurements proportional to the real and imaginary parts of the cross-spectrum, respectively, on the two meters (Ref. 12).

The subject for the experiments was a Navy test pilot stationed at the Naval Air Test Center, Patuxent River, Maryland. He was thoroughly trained on each of the dynamic configurations to achieve a nearly stationary level of performance. For the data runs the conditions were presented several times in a randomized order to minimize any effects due to order of presentation. The actual order used is apparent in Fig. 17. Although only one subject was used for the entire series, two efforts were made to enhance the generality of the results. The first was to use spot checks on certain configurations performed by two other Navy test pilots. The results obtained from these checks were in general agreement with the data for the first subject. The second was a careful tie-in of the data with previous single-loop results. These two efforts were intended to be accomplished only with Configuration A; however, the outer loop measurements in the other configurations also showed remarkably good agreement with some of the single-loop experimental data. This will be discussed in the subsection on outer loop control behavior.

Inner Loop Control Behavior

As noted earlier, if the crossfeed is absent the pilot describing functions in the yaw rate loop, Y_r, can be measured directly from the simple ratio of cross-spectra,

$$Y_r = \frac{\Phi_{\varphi_c \delta_r}}{\Phi_{\varphi_c r}} \tag{9}$$

whereas with cross-control the same cross-spectral ratio contains two pilot describing functions which cannot be separated, i.e.,

$$\frac{\Phi_{\varphi_c \delta_r}}{\Phi_{\varphi_c r}} = \frac{Y_r\left(\frac{r}{\delta_a}\right) + Y_{cf}}{\left(\frac{r}{\delta_a}\right) + Y_{cf}\left(\frac{r}{\delta_r}\right)} \tag{10}$$

An examination of the data on this cross-spectral ratio clearly indicated that the pilot was cross-controlling in the multiloop configurations. For instance, the data for Configuration B, shown in Fig. 11,* cannot be fitted by

*The small circles indicate the means of several runs, the short horizontal lines indicate the means plus or minus one standard deviation, and the small numbers at the top of the figure indicate the number of runs which were averaged for each frequency point. The number of runs is not the same for all frequencies because each run generally consisted of recording bank angle data at five frequencies and yaw rate data at the other five frequencies. Simultaneous recording of bank angle and yaw rate data at all ten frequencies was not possible because of the limited number of watthour meters available.

the simple describing function form which would be estimated to represent pilot closure of a yaw-rate-to-rudder loop on a single-loop basis. We therefore used a composite of three different methods to find values for the pilot crossfeed and yaw-rate-to-rudder describing functions which were both physically reasonable and compatible with the data.

The first technique was to assume for either the crossfeed, Y_{cf}, or yaw-rate-to-rudder, Y_r, describing function and to solve for the other describing function from the equation

$$\Phi_{\varphi_c\delta_r} = Y_r\Phi_{\varphi_c r} + Y_{cf}\Phi_{\varphi_c\delta_a} \tag{11}$$

The second method used was to assume that the crossfeed and yaw-rate-to-rudder describing functions were constant between adjacent frequency points. Then by taking the cross-spectral data for these frequency points, we effectively had two equations in two unknowns. This unfortunately was not completely successful because it required that the cross-spectra change significantly between frequency points while the pilot describing functions did not change significantly. The third technique used was to attempt to locate frequency regions for the various cross-spectra or ratios of cross-spectra in which the effects of either the crossfeed or the yaw-rate-to-rudder closure would dominate.

Combining the results obtained from all three approaches, the following can be stated:

- The magnitude of the yaw-rate-to-rudder describing function in the region of crossover appears to be about that required to maximize the damping of the closed-loop dutch roll mode
- There definitely was an aileron-to-rudder crossfeed
- The magnitude of this crossfeed near the crossover frequency was roughly that required to cancel the yaw acceleration produced by the ailerons, N'_{δ_a}
- The crossfeed describing function included a low frequency lag/lead which would reduce the cross-coupling effects of N'_p

To reinforce the plausibility of these assumptions, consider Fig. 12.

One curve in Fig. 12 is the pre-experimental estimate made using the single-loop model and adjustment rules to form a yaw rate loop closure with no crossfeed. The experimental data have trends similar to the estimate in certain frequency regions, although the amplitude ratio departs drastically in the frequency region of 0.3 to 1.0 rad/sec and the phase is generally translated to the right. While it is theoretically possible to "resolve" these differences by assigning more equalization to the yaw rate closure, the result would demand an exceedingly complex pilot equalizing capacity which has no precedence. On the other hand, the provision of an aileron-to-rudder crossfeed which tends to cancel the N'_p and N'_{δ_a} aerodynamic cross-coupling has the basic effect of modifying the amplitude ratio and phase in precisely those regions where the pre-experimental estimates depart most drastically from the experimental results. This is shown

in Fig. 12, where the crossfeed is the simple lag/lead noted there. As can be seen, the amplitude fit in the region 0.3 – 1.0 rad/sec is improved considerably, as is the phase fit in the region 1 – 2 rad/sec. The amplitude fit near 4 rad/sec is not as good with the crossfeed in, but that could probably be improved by additional modifications to Y_r and Y_{cf}. Additional rationales for this explanation are provided by the pilot's volunteered subjective impression that this was precisely what he was attempting to do, and by the similarity between pilot action and that often used in automatic flight controls to achieve the same purposes.

Outer Loop Control Behavior

While some difficulty was encountered in the interpretation of the inner loop data, the results for the command (bank angle) loop were quite clear and conclusive. The measured bank-angle-to-aileron describing functions are shown in Figs. 13a – 13c and 14a – 14c. Also shown in the figures are the analytic curve fits made for the describing function data. Values of the describing function parameters for all five configurations are listed in Table II along with similar parameters for the K/s and K/s^2 controlled elements from Ref. 1.

Comparisons of the entries in Table II show the surprising result that the pilot characteristics in the command loop were independent of his behavior in the inner loops, i.e., the pilot describing functions were the same for the stable, slightly unstable, and highly unstable configurations, A, B, and C, respectively. In addition, the outer loop measurements were in very good agreement with the single-loop experiments of Ref. 1. The identical control element was not tested in Ref. 1, but the bank angle tracking task with a stable dutch roll* should fall somewhere between the K/s and K/s^2 experiments of Ref. 1. Not only are the command loop data and the single-loop data of Ref. 1 very similar, but it is, in fact, apparent that the pilot describing function model and adjustment rules of Ref. 1 can be carried over directly to the control of command loops in multiloop systems.

Particularly noteworthy in Table II are the values of the pilot lead time constant, T_L, for all the configurations with input bandwidth of 1.6 rad/sec or below (A through D). This is set to almost exactly cancel the roll subsidence time constant, T_R. For the larger bandwidth situation, T_L is increased. Because the crossover frequency is unchanged, this has the effect of increasing the phase margin, which in turn results in a decrease in tracking error under that which would be present if the change was not made. This effect coincides with its single-loop equivalent described in Ref. 1.

The values for crossover frequency and phase margin were obtained from the measured cross-spectra of input and bank angle error. These cross-spectra can be written

$$\Phi_{\varphi_c \varphi_e} = \frac{1}{1 + Y_\varphi (\varphi/\delta_a)_{eff}} A_c \qquad (12)$$

where $(\varphi/\delta_a)_{eff}$ is the effective bank-angle-to-aileron transfer function, i.e., the φ/δ_a response with all pilot inner loops closed, and A_c is the amplitude of

*Bank-angle-to-aileron response is closely approximated by $K/s(T_R s + 1)$, where T_R = 0.2 sec.

an input wave. The effective open-loop describing function, $Y_{\varphi}(\varphi/\delta_a)_{eff}$, was computed from Eq. 12 using the measured command bank angle error cross-spectra $\Phi_{\varphi_c\varphi_e}$. These are shown in Figs. 15a – 15c and 16a – 16c. These figures show that the pilot was able to use the inner loops to keep the effective bank-angle-to-aileron response invariant with changes in dutch roll stability.

The curves superimposed on the data of Figs. 15 and 16 illustrate the application of the simple crossover model to these situations. This most simple of human pilot models, which was evolved originally for very simple controlled elements, is seen to be reasonably valid in these far more complicated multiloop situations.

Performance Measures and Pilot Ratings

The describing function results discussed above also correlate with the measured tracking performance. Figure 17 shows the rms tracking errors for all the data runs (practice runs made the first day of the tests are not shown). The tracking performance for Configurations A (stable) and B (slightly unstable) are essentially the same, while the errors for Configuration C (highly unstable) appear slightly less. Thus, of these three the pilot did the best tracking when he was working the hardest in the inner loops. The error trend with input bandwidth is as expected, increasing input bandwidth (Configurations D, B, and E) increased tracking errors.

The rms error data also correlate fairly well with the one-third law (Ref. 1), i.e., $\sigma_{\varphi_e}/\sigma_{\varphi_c} \doteq 1/\sqrt{3}\ \omega_i/\omega_c$. The one-third law predicts

$$\frac{\sigma_{\varphi_e}}{\sigma_{\varphi_c}} \doteq \begin{cases} -11 \text{ dB for Configurations A, B, and C} \\ -13 \text{ dB for Configuration D} \\ -7 \text{ dB for Configuration E} \end{cases}$$

The rms yaw rate is shown in Fig. 18. The variation with dutch roll mode stability is as would be expected — yaw rate increases as the dutch roll instability is increased. The variation with input bandwidth is somewhat peculiar, as the yaw rates for Configurations D and E are both larger than that for Configuration B.

One final bit of data worthy of note is the pilot ratings. The severe degradation in pilot rating as the dutch roll instability was increased is shown below.

Configuration	Pilot Rating (Cooper Scale)
A (stable)	4
B (slightly unstable)	6
C (highly unstable)	8

The less severe effects of input bandwidth are shown by:

Configuration	Input Bandwidth (rad/sec)	Pilot Rating (Cooper Scale)
D	1.2	5.5
B	1.6	6
E	2.4	7

The pilot rating for Configuration A can be compared with the roll control experiments of Ref. 11. In those experiments a configuration of $T_R = 0.2$ sec was rated 1 – 2.5 when the control sensitivity was optimum (in our experiments the pilot was allowed to select the control sensitivity). The poorer rating for Configuration A is apparently due to the magnitude and frequency content of the command input (the Ref. 11 experiments did not include an input).

CONCLUSIONS

Both general and specific conclusions can be drawn from the data and analyses presented here. The specific conclusions are given in the individual sections, so only the general conclusions are summarized below.

- For multiloop control situations with an integrated display, the quasi-linear pilot model and adjustment rules evolved for single-loop systems are applicable to the multiloop system command loop.
- The single-loop pilot model is also applicable, with reservations, to inner loop closures.
- When it is advantageous to do so, a pilot will adopt a control crossfeed to reduce the inadvertent excitations of a subsidiary or nuisance mode.
- Even while providing both crossfeed and inner loop damping, pilot performance in the command loop — as measured by his describing function and rms errors — can be as good as that in a single-loop task. His subjective opinion, however, will be severely degraded.
- When several feedback possibilities are present in a multiloop situation, the pilot will select those which permit the best dynamic performance with least pilot effort.

ACKNOWLEDGMENT

This paper presents the results of research supported by the Man/Machine Integration Branch, Ames Research Center, National Aeronautics and Space Administration, under Contract NAS2-1868-3. The authors wish to acknowledge the efforts of Mr. W. C. Reisener, Jr., of The Franklin Institute, who provided invaluable contributions to the experiments and data reduction.

REFERENCES

1. McRuer, Duane, Dunstan Graham, Ezra Krendel, and William Reisener, Jr., Human Pilot Dynamics in Compensatory Systems — Theory, Models, and Experiments with Controlled Element and Forcing Function Variations, AFFDL-TR-65-15, Jan. 1965.

2. Cromwell, C. H., and I. L. Ashkenas, A Systems Analysis of Longitudinal Piloted Control in Carrier Approach, Systems Technology, Inc., Tech. Rept. 124-1, June 1962.

3. Ashkenas, I. L., and T. S. Durand, "Simulator and Analytical Studies of Fundamental Longitudinal Control Problems in Carrier Approach," AIAA Simulation for Aerospace Flight Conference, August 1963, pp. 16-34.

4. Durand, T. S., Theory and Simulation of Piloted Longitudinal Control in Carrier Approach, Systems Technology, Inc., Tech. Rept. 130-1, Sept. 1963.

5. Stapleford, R. L., D. E. Johnston, G. L. Teper, and D. H. Weir, Development of Satisfactory Lateral-Directional Handling Qualities in the Landing Approach, NASA CR-239, July 1965.

6. Stapleford, R. L., J. Wolkovitch, R. E. Magdaleno, C. P. Shortwell, and W. A. Johnson, An Analytical Study of V/STOL Handling Qualities in Hover and Transition, AFFDL-TR-65-73, May 1965.

7. Hall, I. A. M., Effects of Controlled Element on the Human Pilot, WADC-TR-57-509, Aug. 1958.

8. McRuer, D. T., and E. S. Krendel, Dynamic Response of Human Operators, WADC-TR-56-524, Oct. 1957.

9. Seckel, E., I. A. M. Hall, D. T. McRuer, and D. H. Weir, Human Pilot Dynamic Response in Flight and Simulator, WADC-TR-57-520, Oct. 1957.

10. Ashkenas, I. L., and D. T. McRuer, Approximate Airframe Transfer Functions and Application to Single Sensor Control Systems, WADC-TR-58-82, June 1958.

11. Creer, B. Y., J. D. Stewart, R. B. Merrick, and F. J. Drinkwater, III, A Pilot Opinion of Lateral Control Requirements for Fighter-Type Aircraft, NASA Memo 1-29-59A, Mar. 1959.

12. Seltzer, L. J., and D. T. McRuer, Survey of Analog Cross Spectral Analyzers, WADC-TR-59-241, Dec. 1959.

13. McRuer, D. T., and D. Graham, Pilot Models for Single- and Multi-loop Systems with Random Forcing Functions, Systems Technology, Inc., Tech. Rept. 134-1 (The Franklin Institute Rept. STI-FIL 5), Nov. 1964.

TABLE I

TESTED CONFIGURATIONS

CONFIGURATION	INPUT BANDWIDTH (rad/sec)	INVERSE TIME CONSTANTS (sec^{-1})		DUTCH ROLL MODE	
		Spiral Mode	Roll Subsidence Mode	Damping Ratio	Undamped Natural Frequency
A	1.6	0.20	5.0	0.75	0.87
B	1.6	0	5.0	-0.075	1.03
C	1.6	-0.054	5.0	-0.35	1.01
D	1.2	0	5.0	-0.075	1.03
E	2.4	0	5.0	-0.075	1.03

TABLE II

COMMAND LOOP CHARACTERISTICS

CONFIGURATION	INPUT BANDWIDTH (rad/sec)	α (rad/sec)	τ_e (sec)	T_L (sec)	CROSSOVER FREQUENCY (rad/sec)	PHASE MARGIN (deg)
A (stable).....	1.6	0.20	0.29	0.20	3.2	20
B (slightly unstable).....	1.6	0.20	0.29	0.20	3.2	20
C (highly unstable).....	1.6	0.20	0.29	0.20	3.2	20
D (slightly unstable).....	1.2	0.20	0.29	0.20	3.2	20
E (slightly unstable).....	2.4	0.20	0.29	0.31	3.2	34
K/s (Ref. 1).....	1.5	0.14	0.24	0	4.6	24
K/s (Ref. 1).....	2.5	0.11	0.18	0	4.7	42
K/s^2 (Ref. 1).....	1.5	0.20	0.39	5	3.2	16
K/s^2 (Ref. 9).....	2.5	0.33	0.34	5	3.3	26

Pilot describing function = $K_p(j\omega T_L + 1)e^{-j(\alpha/\omega + \omega\tau_e)}$

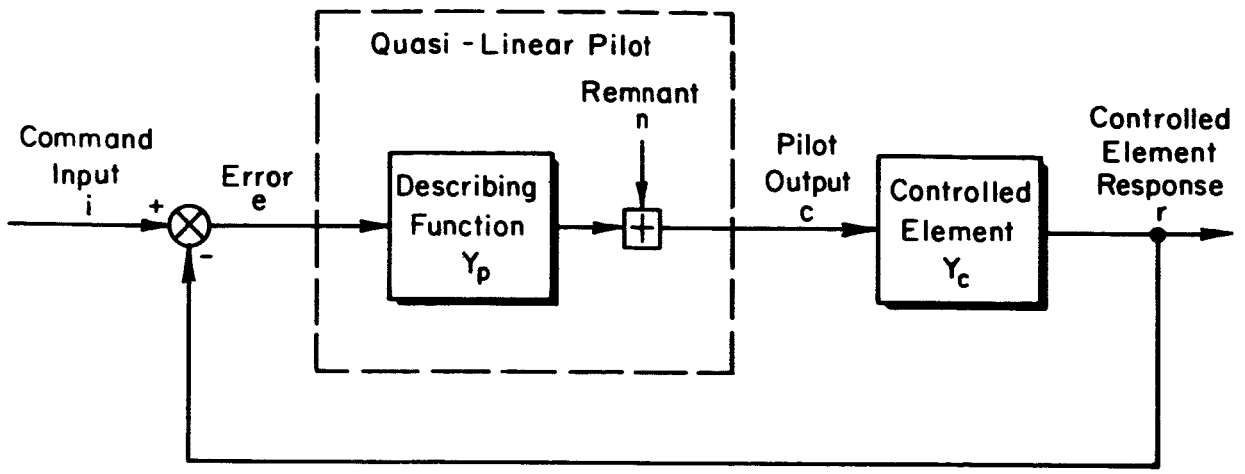

Figure 1. Quasi-Linear Model for a Single-Loop Compensatory System

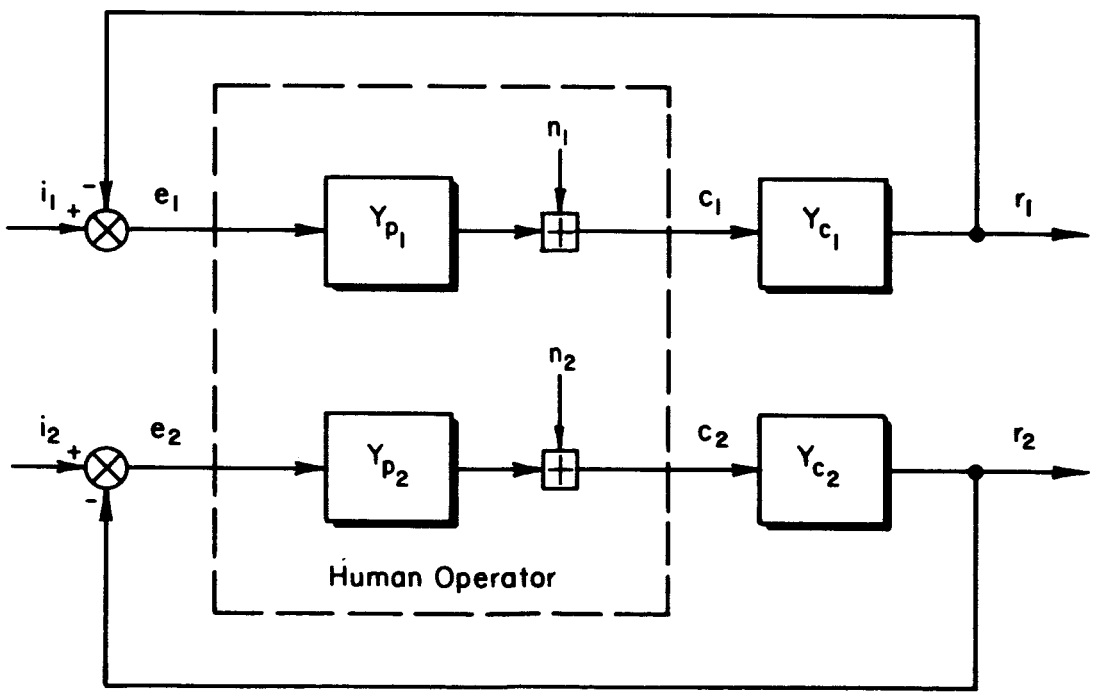

Figure 2. Multiple Single-Loop Manual Control System

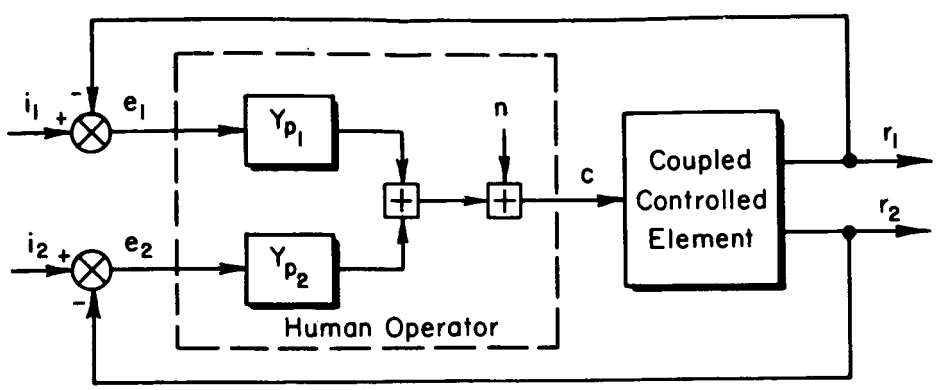

a) Single - Point Controller

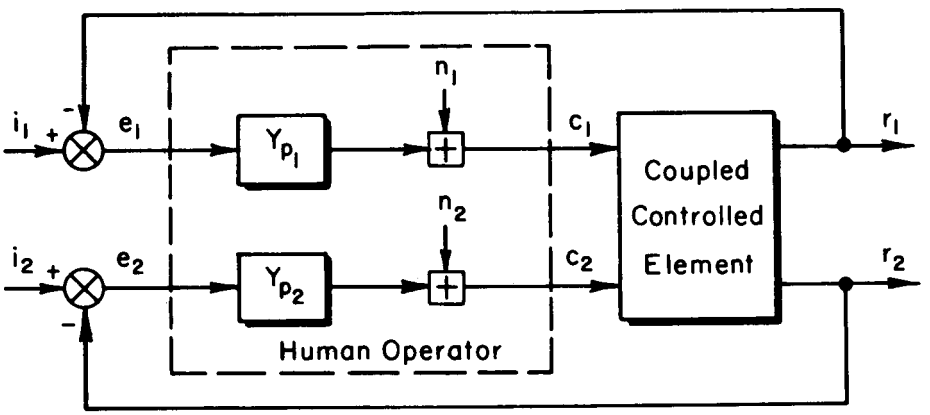

b) Direct Multipoint Controller

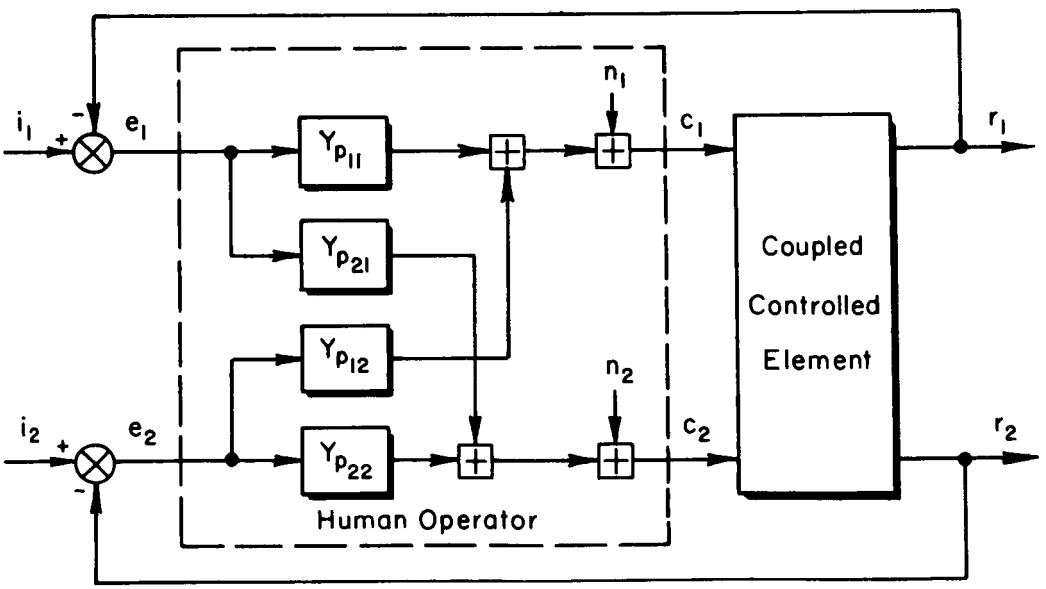

c) Cross - Fed Multipoint Controller

Figure 3. Examples of Multiloop Manual Control System

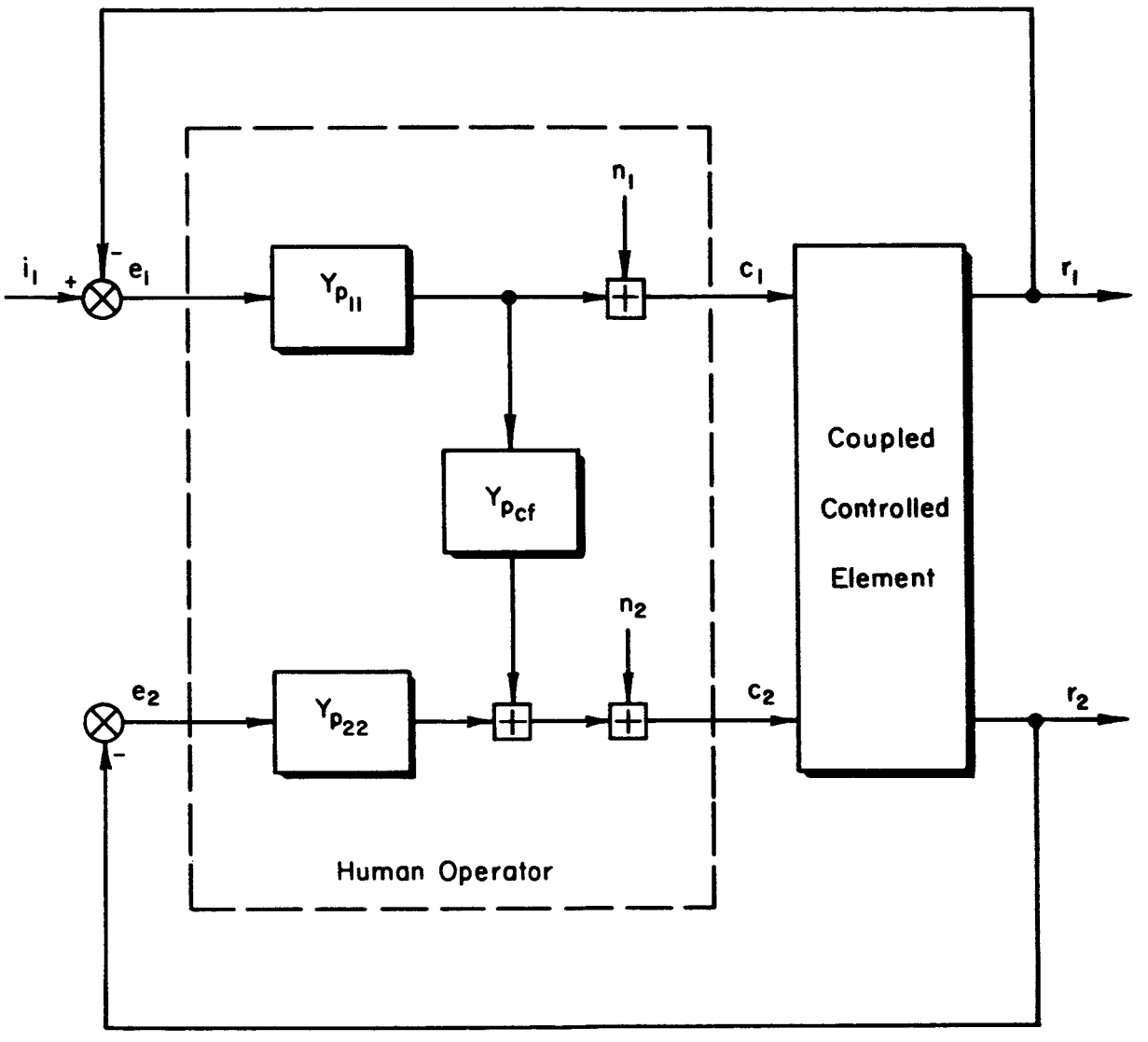

Figure 4. Multipoint Control System with One Crossfeed

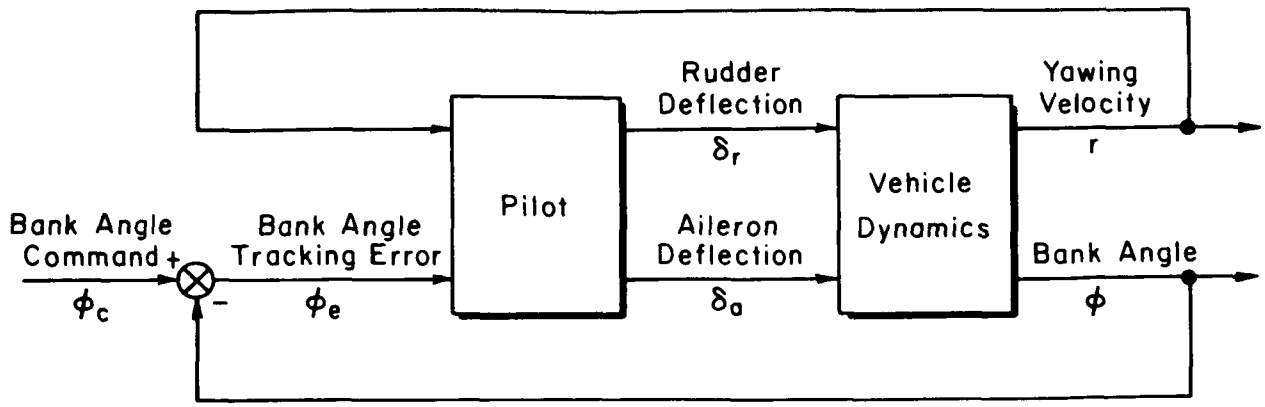

(a) Block Diagram of Bank Angle Tracking Multiloop Control Task

$$\text{Side Acceleration:} \quad s\beta - \frac{g}{U_0}\phi + r = 0 + 0$$

$$\text{Rolling Acceleration:} \quad -L'_\beta \beta + s(s - L'_p)\phi - L'_r r = 0 + L'_{\delta_a}\delta_a$$

$$\text{Yawing Acceleration:} \quad -N'_\beta \beta - N'_p s\phi + (s - N'_r)r = N'_{\delta_r}\delta_r + N'_{\delta_a}\delta_a$$

(b) Vehicle Equations of Motion (Ref. 10)

Figure 5. Multiloop Control Task

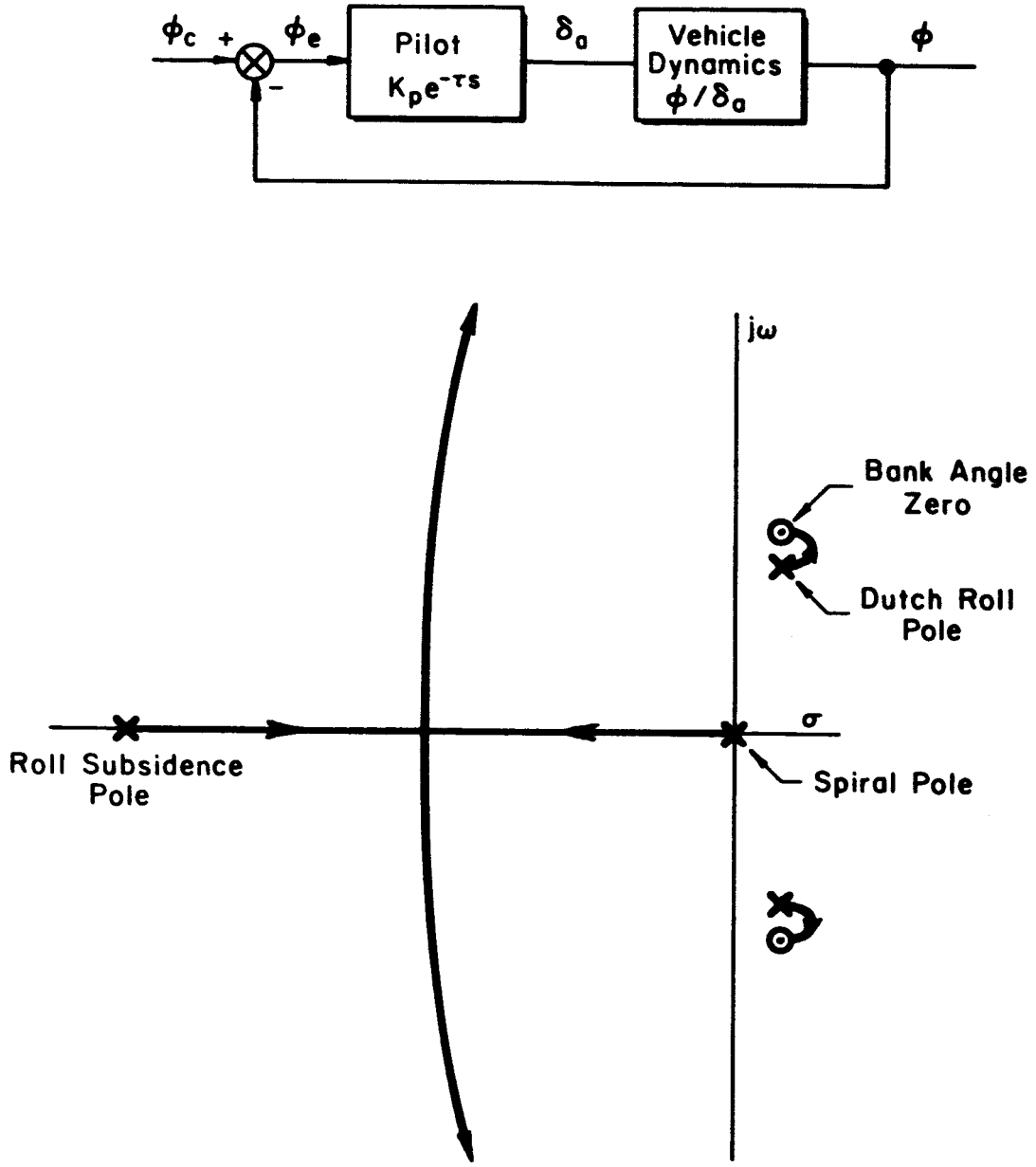

Figure 6. Root Locus of Bank-Angle-to-Aileron Closure for Unstable Dutch Roll Mode

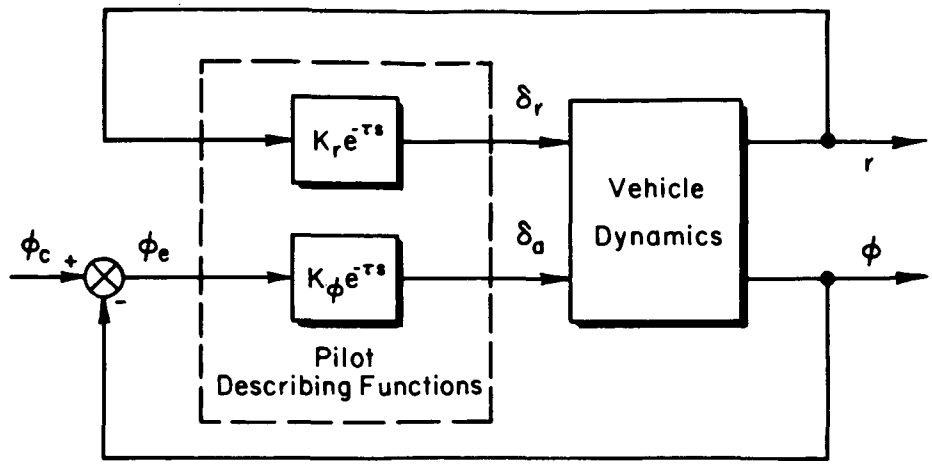

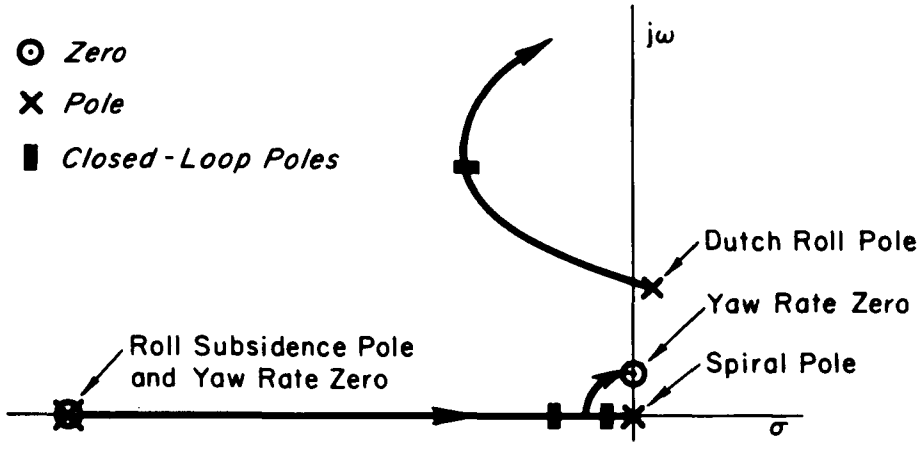

a) Yaw Rate-to-Aileron Inner Loop

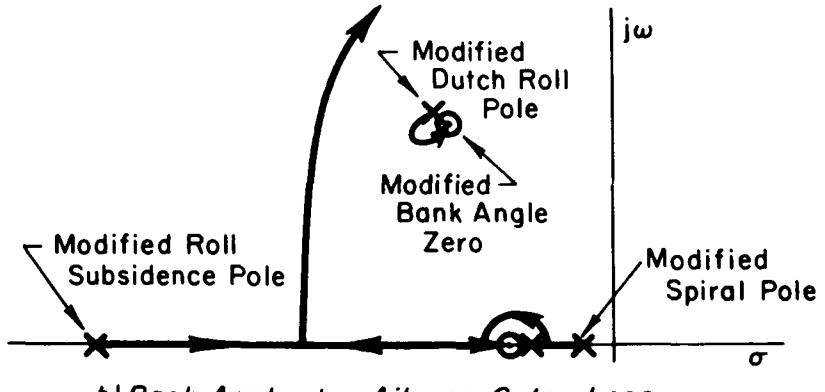

b) Bank Angle-to-Aileron Outer Loop (as modified by yaw rate inner loop)

Figure 7. Root Loci for Pilot Closures of Rudder and Aileron Loops

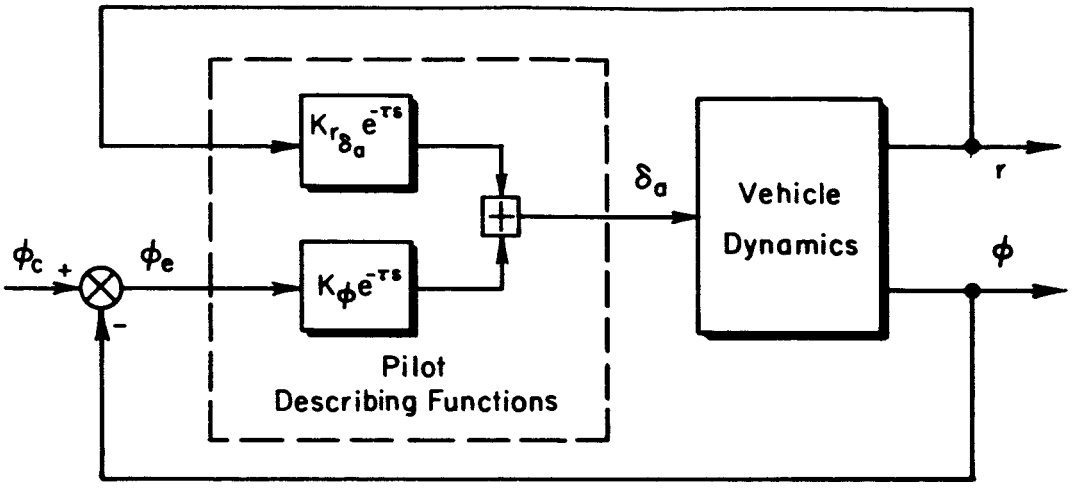

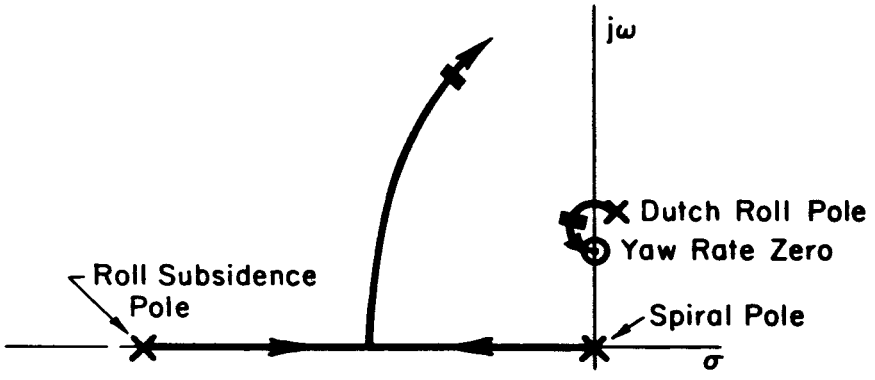

b) Yaw Rate -to- Aileron Inner Loop

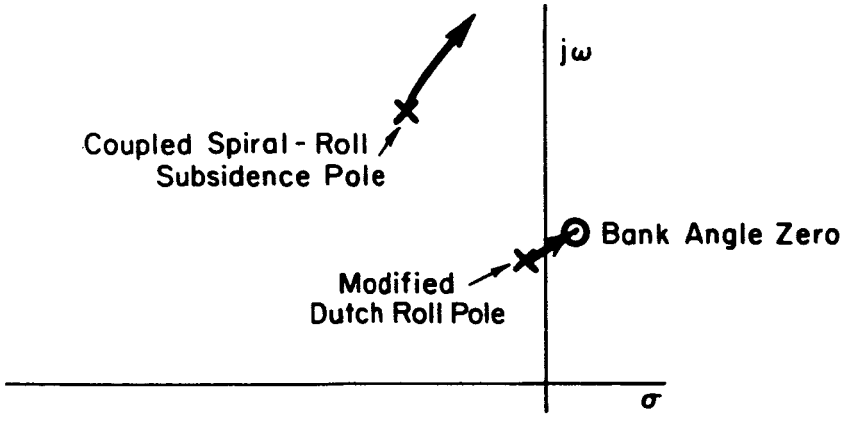

c) Bank Angle -to - Aileron Outer Loop

Figure 8. Root Loci for Pilot Closure of Aileron Alone Loops

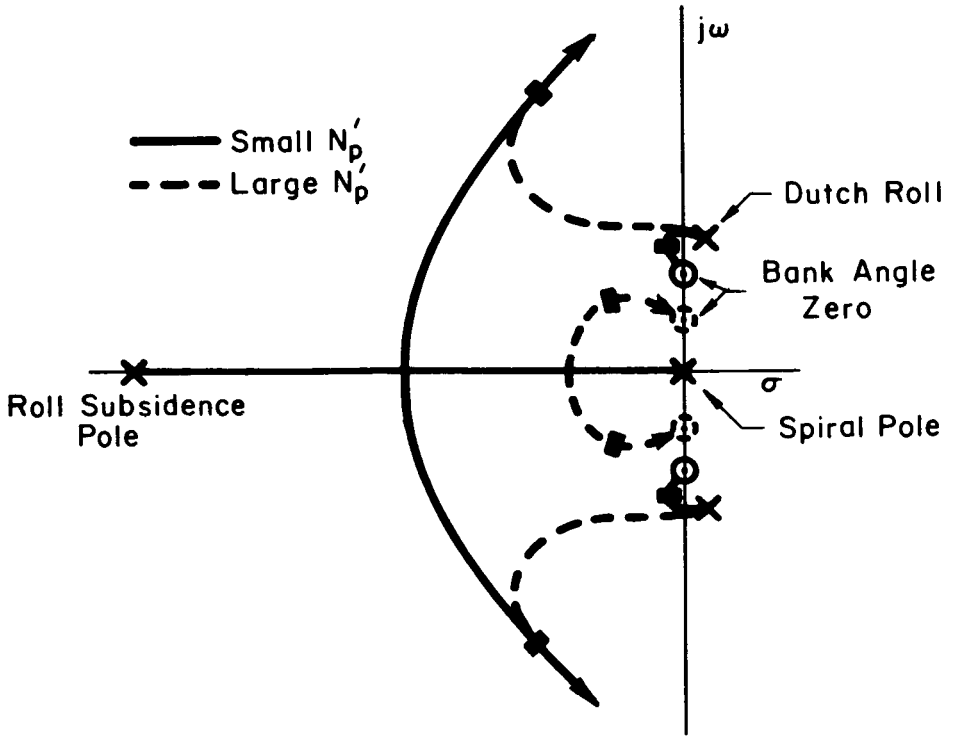

Figure 9. Effects of N_p' on Yaw-Rate-to-Aileron Closure

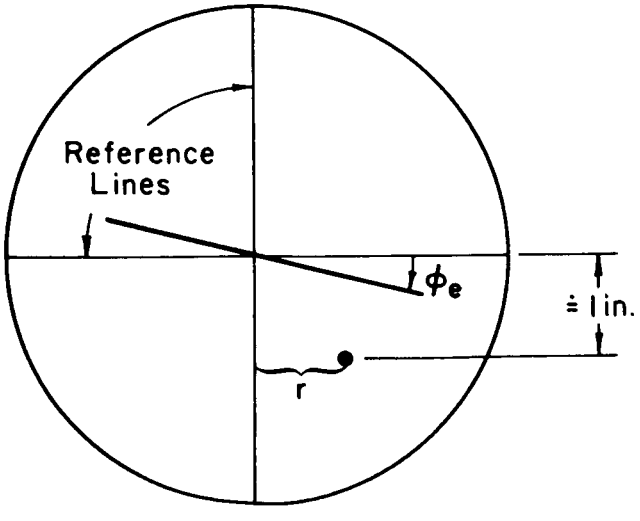

Figure 10. Display

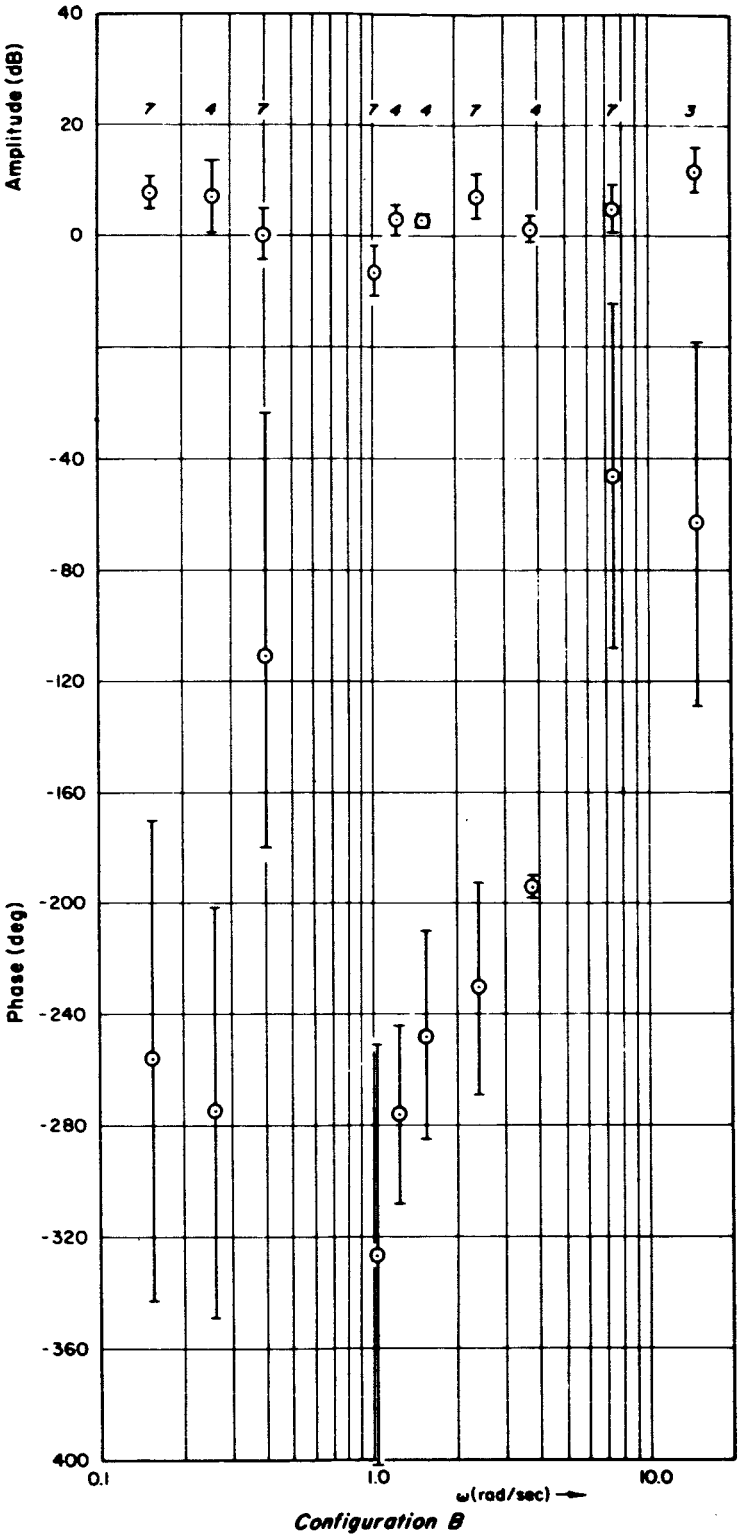

Figure 11. Measured Cross-Spectral Ratio $\Phi_{\varphi_c \delta_r}/\Phi_{\varphi_c r}$

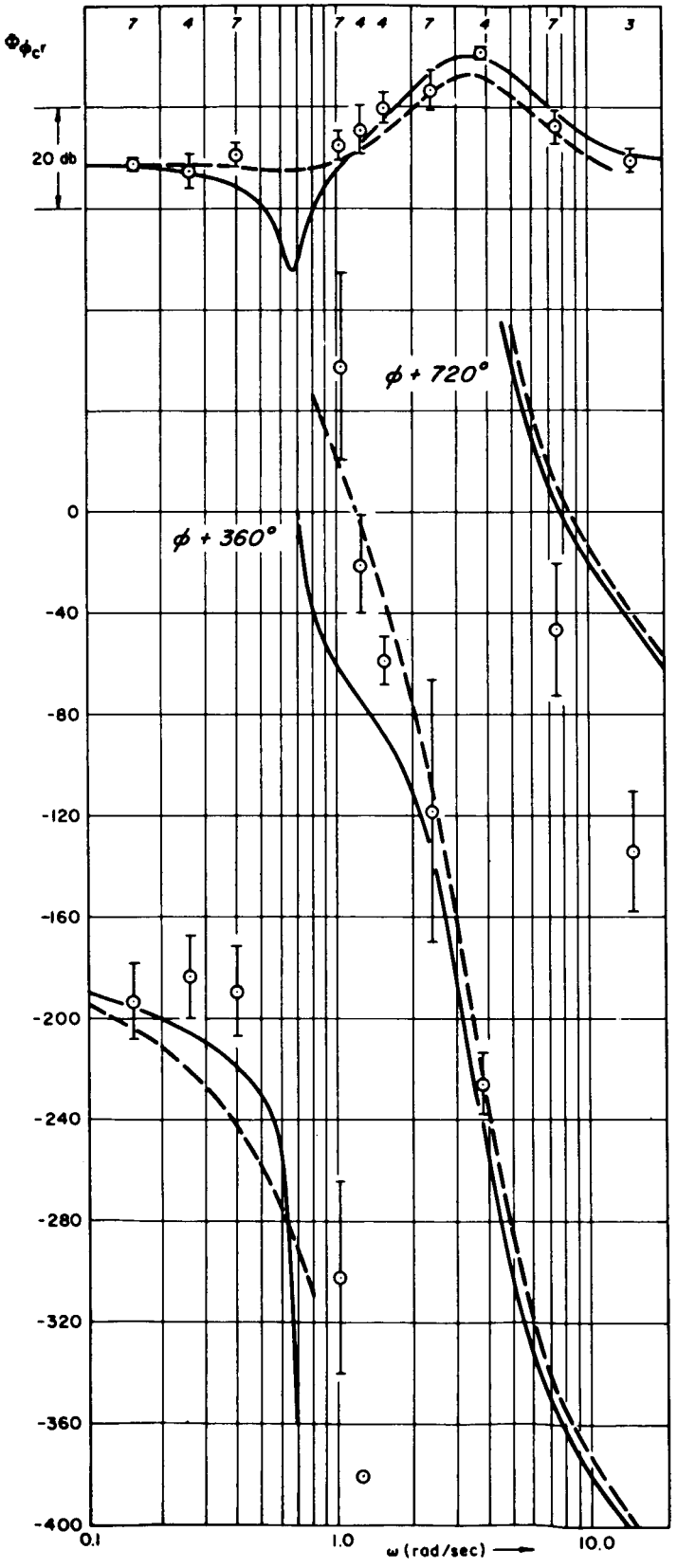

$$Y_{cf} = \frac{-0.5 \frac{N'_{\delta_a}}{N'_{\delta_r}}(s+2)}{(s+0.3)}$$

——— No Crossfeed

– – – With Crossfeed (Y_{cf})

Figure 12. Effect of Crossfeed on Yaw Rate Response

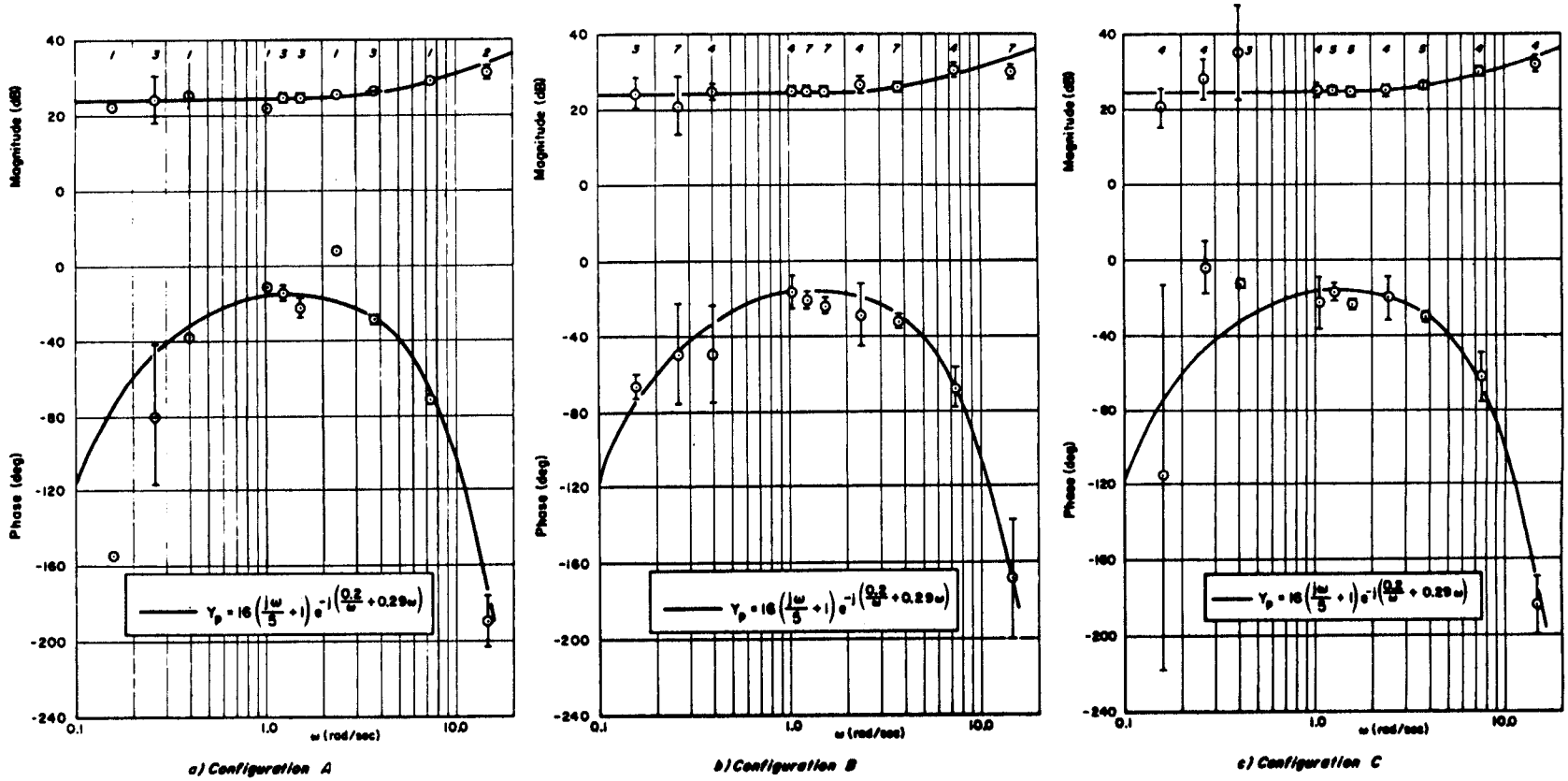

Figure 13. Pilot Command Loop Describing Functions

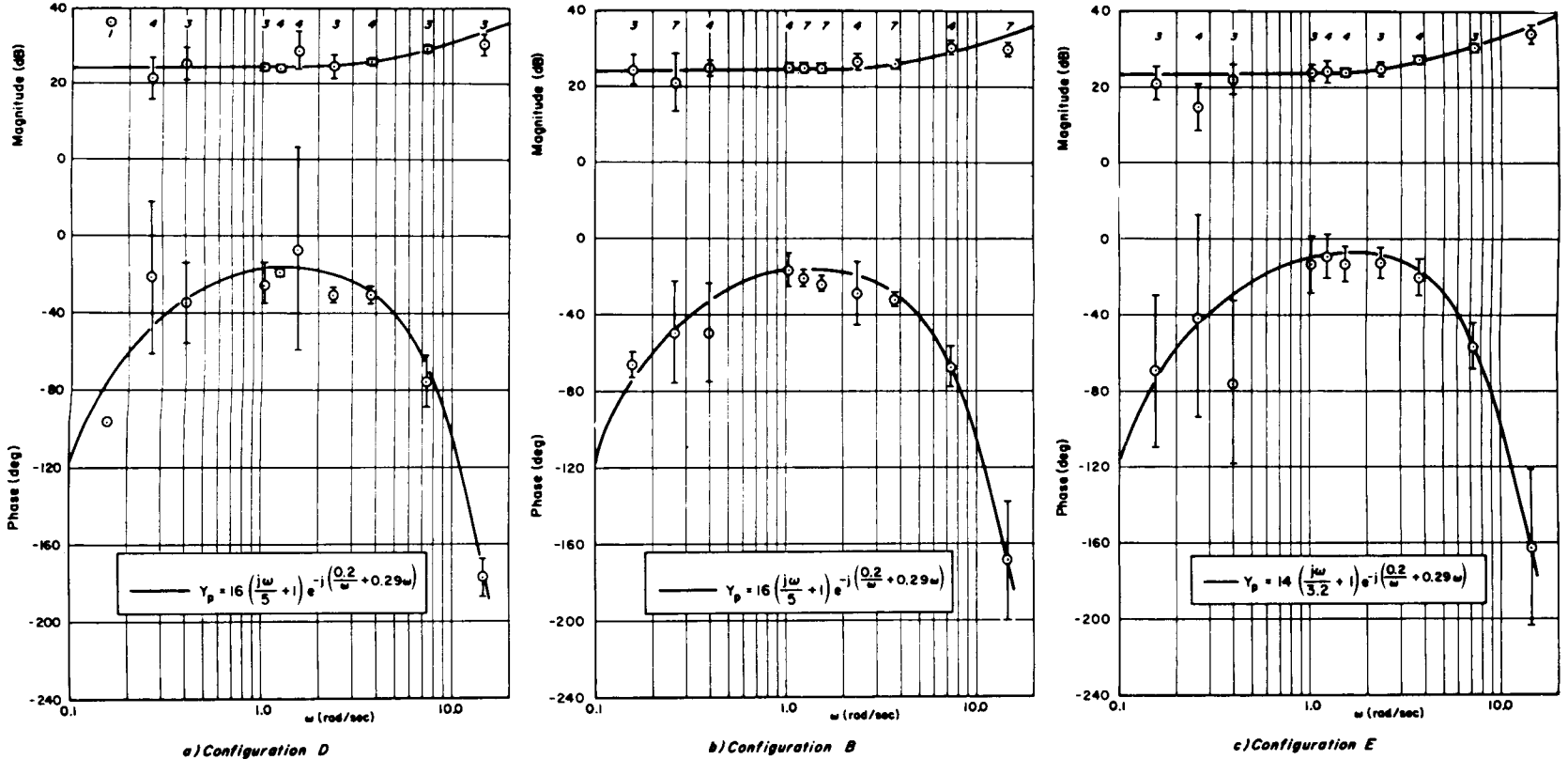

Figure 14. Pilot Command Loop Describing Functions

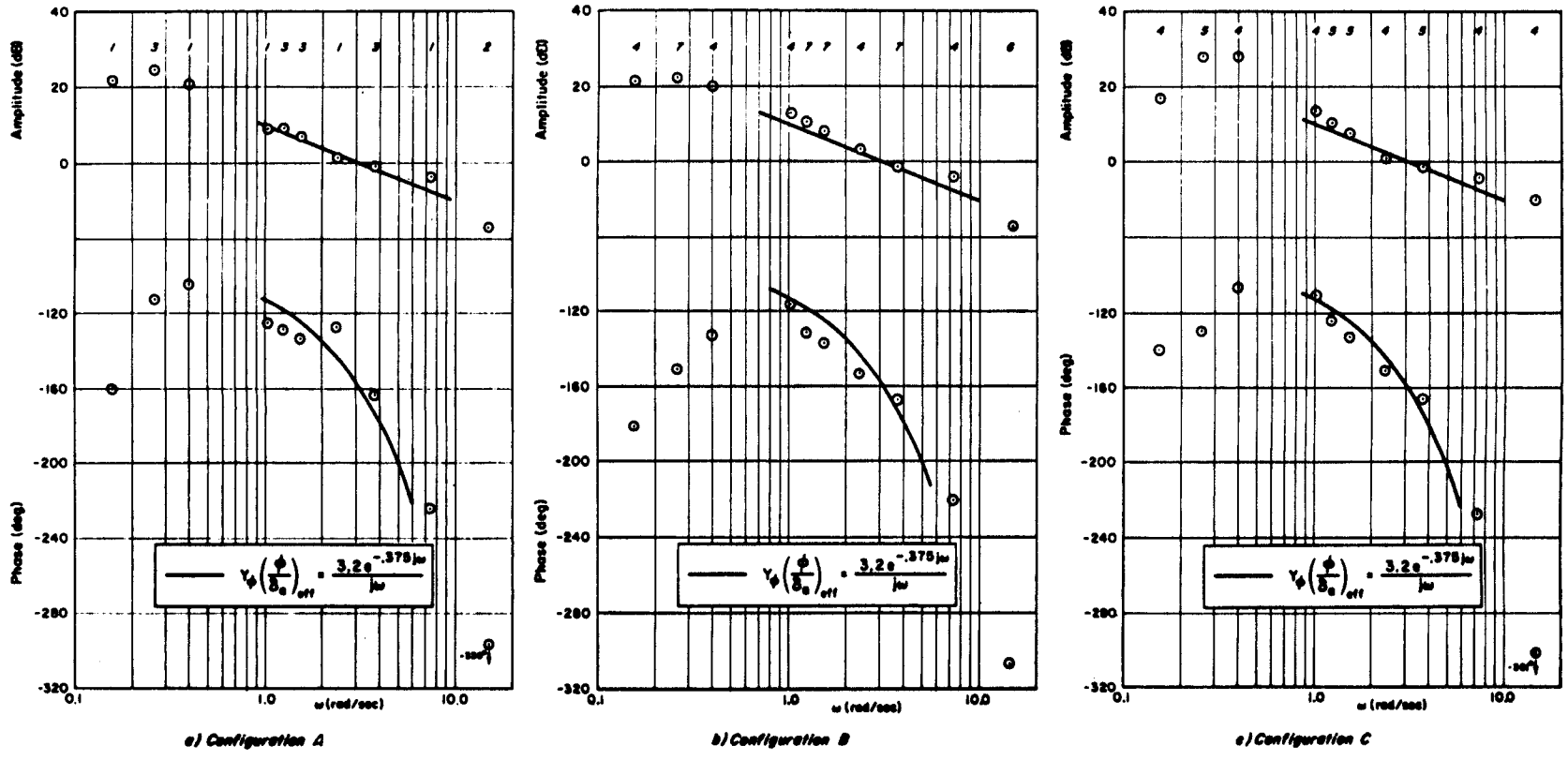

Figure 15. Effective Open-Loop Transfer Function $Y_\varphi(\varphi/\delta_a)_{eff}$

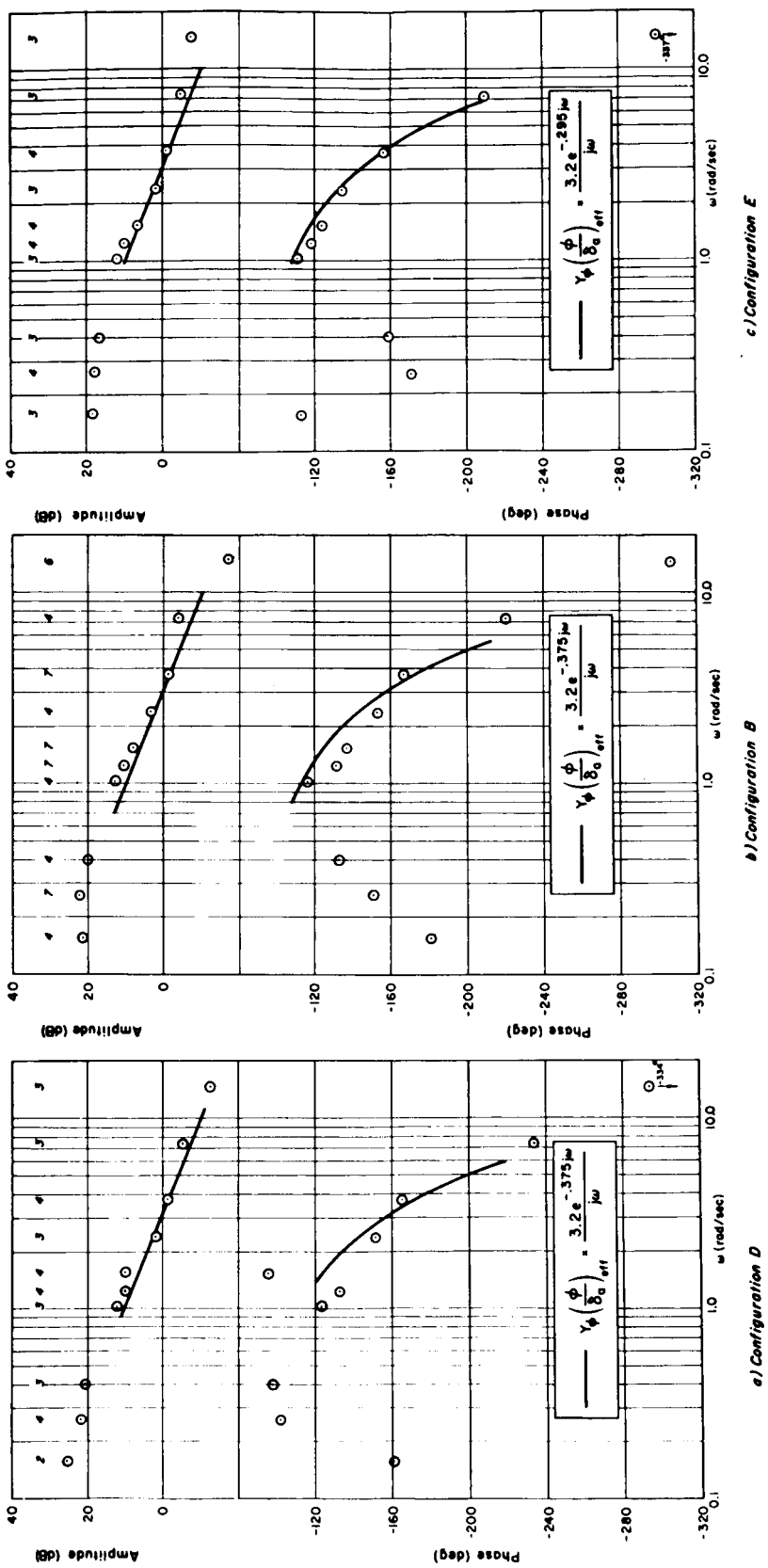

Figure 16. Effective Open-Loop Transfer Function $Y_{\varphi}(\varphi/\delta_a)_{eff}$

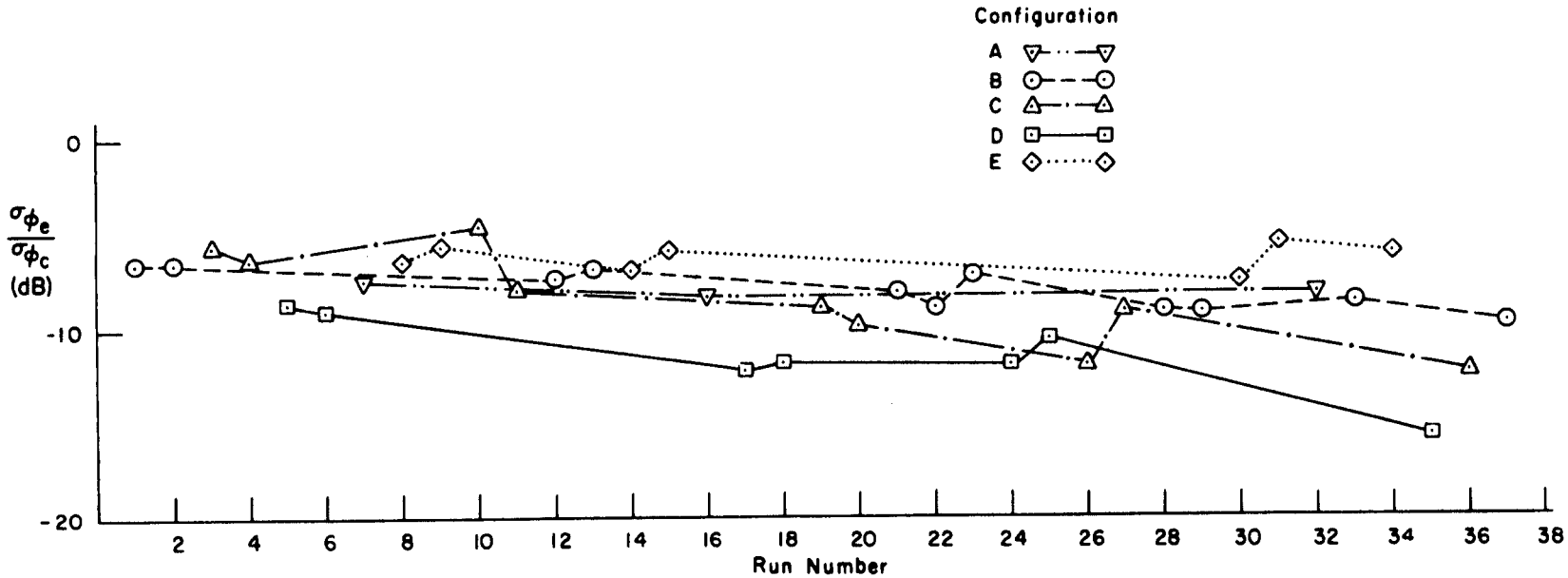

Figure 17. Relative RMS Tracking Errors, σ_i = 11 Deg

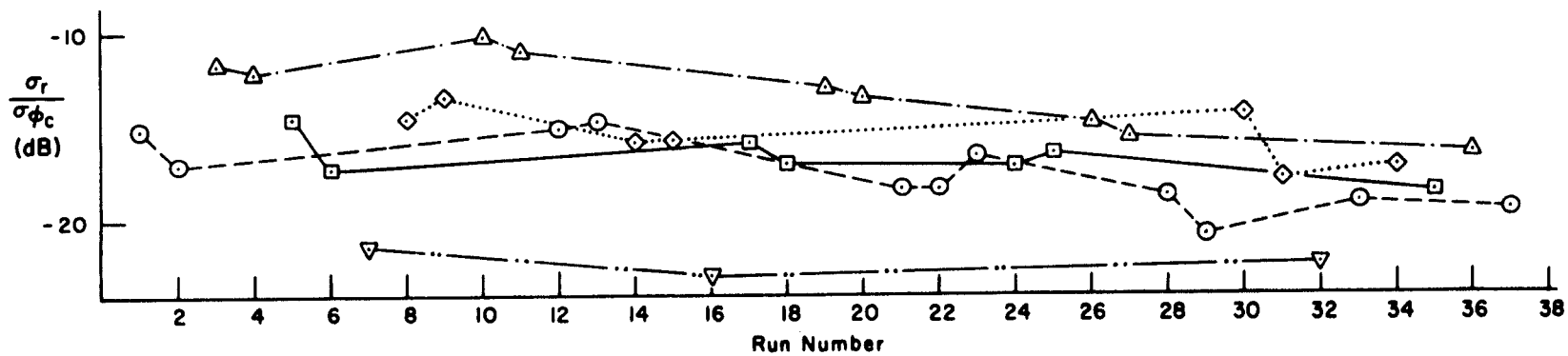

Figure 18. Relative RMS Yaw Rate, σ_i = 11 Deg

APPENDIX

The numerical values of the stability derivatives used in the main experiments are:

$$L'_\beta = -10 \text{ sec}^{-2}$$

$$N'_\beta = 1.0 \text{ sec}^{-2}$$

$$g/U_o = 0.046 \text{ sec}^{-1}$$

$$L'_p = -5.0 \text{ sec}^{-1}$$

$$N'_p = 0.02 \text{ sec}^{-1}$$

$$L'_r = -1.5 \text{ sec}^{-1}$$

$$N'_r = \begin{cases} -1.5 \text{ sec}^{-1} & \text{for Configuration A} \\ 0.15 \text{ sec}^{-1} & \text{for Configurations B, D, and E} \\ 0.75 \text{ sec}^{-1} & \text{for Configuration C} \end{cases}$$

$$N'_{\delta_a}/L'_{\delta_a} = 0.02$$

L'_{δ_a}, N'_{δ_r} (pilot selected the control gains)

The pertinent open-loop transfer functions can be written in the form:

$$\frac{\varphi}{\delta_a} = \frac{L'_{\delta_a}\left(s^2 + 2\zeta_\varphi \omega_\varphi s + \omega_\varphi^2\right)}{\Delta}$$

$$\frac{\varphi}{\delta_r} = \frac{N'_{\delta_r} L'_r \left(s + 1/T_\varphi\right)}{\Delta}$$

$$\frac{r}{\delta_a} = \frac{N'_{\delta_a}\left(s + 1/T_{r_a}\right)\left(s^2 + 2\zeta_{r_a}\omega_{r_a} s + \omega_{r_a}^2\right)}{\Delta}$$

$$\frac{r}{\delta_r} = \frac{N'_{\delta_r}\left(s + 1/T_{r_r}\right)\left(s^2 + 2\zeta_{r_r}\omega_{r_r} s + \omega_{r_r}^2\right)}{\Delta}$$

where $$\Delta = \left(s + 1/T_s\right)\left(s + 1/T_R\right)\left(s^2 + 2\zeta_d\omega_d s + \omega_d^2\right)$$

Numerical values of the transfer function factors are tabulated below.

Factor	Units	Configuration		
		A	B, E, E	C
$1/T_s$	sec^{-1}	0.199	0	-0.054
$1/T_R$	sec^{-1}	5.00	5.00	5.01
ζ_d	———	0.746	-0.075	-0.347
ω_d	rad/sec	0.873	1.025	1.012
ζ_φ	———	0.671	-0.082	-0.356
ω_φ	rad/sec	1.095	1.095	1.095
$1/T_\varphi$	sec^{-1}	←	-6.67	→
$1/T_{r_a}$	sec^{-1}	←	6.07	→
ζ_{r_a}	———	←	-0.055	→
ω_{r_a}	rad/sec	←	0.674	→
$1/T_{r_r}$	sec^{-1}	←	5.02	→
ζ_{r_r}	———	←	-0.030	→
ω_{r_r}	rad/sec	←	0.303	→